SCIENCE CHINA
Physics, Mechanics & Astronomy

•Article•

June 2022 Vol. 65 No. 6: 264613
https://doi.org/10.1007/s11433-021-1878-4

Unraveling the threshold stress of structural rejuvenation of metallic glasses via thermo-mechanical creep

Gan Ding[1,2], Feng Jiang[1], Xuan Song[2,3], LanHong Dai[2,3], and MinQiang Jiang[2,3*]

[1] *State Key Laboratory for Mechanical Behavior of Materials, Xi'an Jiaotong University, Xi'an 710049, China;*
[2] *State Key Laboratory of Nonlinear Mechanics, Institute of Mechanics, Chinese Academy of Sciences, Beijing 100190, China;*
[3] *School of Engineering Science, University of Chinese Academy of Sciences, Beijing 100049, China*

Received December 7, 2021; accepted February 23, 2022; published online April 29, 2022

The competition between physical aging and structural rejuvenation determines the physical and mechanical properties of glassy materials. Thus, the rejuvenation-aging boundary must be identified quantitatively. In this work, we unravel a stress boundary to distinguish rejuvenation from aging via the thermo-mechanical creep of a typical Zr-based metallic glass. The crept glasses were rejuvenated into high-enthalpy disordered states when the applied stress exceeded a threshold that was numerically close to the steady-state flow stress; otherwise, the glasses were aged. A theoretical model for glass creep was adopted to demystify the observed stress threshold of rejuvenation. The model revealed that the thermo-mechanical creep beyond the threshold stress could activate sufficient shear transformations to create a net free volume, thus leading to structural rejuvenation. Furthermore, we derived the analytical expressions for the threshold and flow stresses. Both stresses can act as the rejuvenation-aging boundary, which is well supported by experimental creep data. The present work procures a deeper understanding of the rejuvenation mechanism of glasses and provides useful implications for abstaining from glass aging.

metallic glass, thermo-mechanical creep, threshold stress, shear transformations, rejuvenation-aging boundary

PACS number(s): 71.23.Cq, 62.20.Hg, 81.40.Jj, 62.20.F-, 71.55.Jv

Citation: G. Ding, F. Jiang, X. Song, L. H. Dai, and M. Q. Jiang, Unraveling the threshold stress of structural rejuvenation of metallic glasses via thermo-mechanical creep, Sci. China-Phys. Mech. Astron. **65**, 264613 (2022), https://doi.org/10.1007/s11433-021-1878-4

1 Introduction

Metallic glasses possess a complex energy landscape and reside in a series of thermodynamically metastable, local basins [1-3]. Their dynamics evolve into two competitive processes: physical aging (ordering) and structural rejuvenation (disordering). The former is generally spontaneous, whereas the latter requires an external energy injection to "shake up" the frozen-in disordered structure [4-7]. Rejuvenated metallic glasses can show enhanced plastic deformability [8-12], which is useful for their engineering applications. Therefore, understanding the rejuvenation of metallic glasses has been the object of intense investigations [13-17].

In general, the degree of structural rejuvenation can be measured by the amount of atomic free volume, which is commonly quantified in terms of the excess exothermic enthalpy before the glass transition. Theories [18-20] and experiments [21] have demonstrated that free volume dynamics are mediated by shear transformations (STs), i.e., localized irreversible rearrangements of small groups of atoms or particles. The structural mechanism for glass rejuvenation thus points toward the net creation of an atomic free volume induced by STs at the nanoscale [22]. Such a trans-scale

*Corresponding author (email: mqjiang@imech.ac.cn)

dynamic process has been revealed by Dmowski and co-workers [23-25] by using high-energy X-ray diffraction (XRD). They further observed that the anelastic strain significantly contributes to rejuvenation. STs are stress-driven and thermally activated events. Therefore, glass rejuvenation is expected to require applied stress beyond a threshold to continuously trigger STs and simultaneously avoid relaxation-induced aging [26,27]. The phenomena of threshold stress have been observed in experiments [23,28] that constructed a stress boundary between rejuvenation and aging. From a practical perspective, however, how to *a prior* determine this stress boundary is still unknown. According to a constitutive model of amorphous plasticity developed previously by Jiang et al. [29], the threshold stress should numerically exceed the steady-state flow stress. However, this theoretical prediction demands direct experimental proof. Furthermore, scientific studies should further understand glass rejuvenation in the unifying theoretical framework of STs and free volume.

In this work, we carried out a series of thermo-mechanical creep experiments on a typical Zr-based bulk metallic glass. The structural and mechanical characterizations of the crept samples confirmed that steady-state flow stress could serve as a guide for the threshold stress of rejuvenation. We further used a theoretical model to describe glass creeps, from which the observed stress threshold was demystified. The model revealed that structural rejuvenation resulted from the ST-mediated net creation (overwhelming annihilation) of free volume, which was only active when the applied creep stress was higher than the threshold or flow stress. Accordingly, the analytical expression of the threshold stress was derived and used to construct the rejuvenation-aging boundary.

2 Material and methods

Given its high glass forming ability and thermal stability, $Zr_{55}Cu_{30}Ni_5Al_{10}$ (at.%) was selected as the representative metallic glass for this study. Rods with a diameter of 5 mm were prepared by suction casting from master alloy ingots to a water-cooled copper mold under a pure argon atmosphere. Cylindrical samples with an aspect ratio of 2:1 were cut from the as-cast rods for the thermo-mechanical creep experiments. To eliminate the difference in thermal history, we pre-annealed all samples at 623 K for 6 h before the creeps. The amorphous structures for as-cast and pre-annealed glasses were verified by XRD (Rigaku Smart Lab 9) with Cu Kα radiation. Calorimetric measurements were performed by differential scanning calorimetry (DSC, TA Q2000) in a pure argon atmosphere at a constant heating rate of 20 K/min. According to the measured DSC curves, the glass transition temperature T_g and crystallization temperature T_x for the as-cast samples were about 683 and 758 K, respectively. For the pre-annealed samples before the creeps, T_g and T_x were about 679 and 757 K, respectively.

The compressive thermo-mechanical creeps were performed on the pre-annealed glasses with a Gleeble 3800 in a vacuum at 553, 603, 623, 643, and 668 K. All temperatures were below T_g to avoid the possible crystallization during the creeps. At each temperature, the applied creep stresses σ_{cp} were set around the steady-state flow stresses σ_f of the glass. As shown in sect. I of Supporting Information, σ_f at different temperatures can be easily determined from the compressive stress-strain curves under a very low strain rate of 1.6×10^{-4} s^{-1}. During the creeps, the samples were first heated to the target temperatures and stabilized for 5 min. Then, the compressive load was applied and held for 20 min at the target temperatures under a constant force mode. During the loading process, the instantaneous creep strain ε_{cp} was recorded directly. All the measured creep strain curves are shown in sect. II of Supporting Information, indicating different creep stresses and temperatures. After the creeps, the samples were immediately quenched to the ambient temperature by high-speed water mist, which can effectively freeze the glassy structures as much as possible. All crept samples retained a completely amorphous structure, which was confirmed by their XRD patterns, as shown in sect. III of Supporting Information. These crept glasses were further characterized by DSC and nanoindentation. Nanoindentation measurements were performed in a Nanovea system equipped with a standard Berkovich diamond tip indenter. We adopted the load-controlled mode: the peak load P_{max} was fixed at 300 mN with a loading rate of 5 mN/s.

3 Results and discussion

3.1 Creep strain

To highlight the action of external stress, we plotted the measured creep strain ε_{cp} with loading time under different applied stresses (Figure 1). Regarding the flow stress σ_f as a reference, these creep curves can be divided into two groups, namely, $\sigma_{cp}>\sigma_f$ and $\sigma_{cp}<\sigma_f$. In 1200 s, all creep strains displayed a two-stage behavior: a sudden jump followed by a very slow or gradual increase. The first strain-jump stage was due to the instantaneous load of creep stress σ_{cp}, whereas the second stage was the strain response of the constant σ_{cp}. The two groups showed different creep behaviors, which are highlighted as green and red lines in Figure 1. For the $\sigma_{cp}<\sigma_f$ group, the creep strain ε_{cp} at the second stage increased very slowly or was almost unchanged. However, for the $\sigma_{cp}>\sigma_f$ group, the second stage exhibited a remarkable increase in the creep strain. Notably, a transition of the creep mechanism occurred when the creep stress σ_{cp} increased across the flow stress σ_f. Such σ_{cp}-dependent creep behaviors were consistent with those of previous works [27,30-32]. The underlying

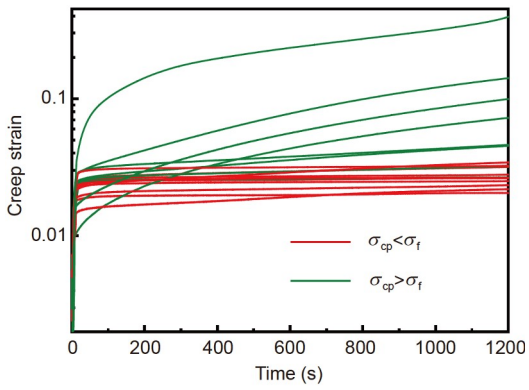

Figure 1 (Color online) Creep strain vs. loading time for different applied stresses.

mechanism is that the creep under low stress is diffusion-controlled, while high stress induces a deformation-controlled creep [32]. Thus, we reasonably speculated that the present creeps of $\sigma_{cp}>\sigma_f$ will enter the strain-divergence stage if the creep time is sufficiently long.

3.2 Excess relaxation enthalpy before T_g

Next, we quantitatively determined whether these crept glasses were structurally rejuvenated or aged. To achieve this objective, we measured the DSC traces of these crept glasses at different temperatures and σ_{cp} normalized by σ_f (Figure 2(a)-(e)). For comparison, the DSC traces of the pre-annealed samples before creeps were also included. Based on the measured DSC traces, the exothermic "excess relaxation enthalpy" (ΔH) before T_g was calculated by numerical integration. We normalized the ΔH_{cp} of the crept glasses by that ΔH_{pr} of the pre-annealed sample before creeps and plotted $\Delta H_{cp}/\Delta H_{pr}$ versus σ_{cp}/σ_f in Figure 2(f). Evidently, if $\Delta H_{cp}/\Delta H_{pr}>1$, then the crept glasses were rejuvenated; otherwise, they were aged. We observed that the rejuvenated glasses ($\Delta H_{cp}/\Delta H_{pr}>1$) resided on the right side of $\sigma_{cp}/\sigma_f=1$ (vertical dashed line). By contrast, the creep-aged glasses belonged to the lower-left red region bounded by $\Delta H_{cp}/\Delta H_{pr}<1$ and $\sigma_{cp}/\sigma_f<1$. In other words, the rejuvenation of crept glasses required a threshold stress, which is consistent with the previous thermo-mechanical creeps [23]. In addition, theoretical results unraveled that low stress makes glasses more homogeneous and denser, but high stress leads to a more heterogeneous and disordered structure [27]. Furthermore, the rejuvenated and aged glasses corresponded exactly to the $\sigma_{cp}>\sigma_f$ and $\sigma_{cp}<\sigma_f$ creeps, respectively. This finding provides direct evidence that the temperature-dependent flow stress σ_f can act as a guide to determine the rejuvenation threshold of thermo-mechanical creeps.

In the rejuvenation green region, at constant σ_{cp}, a high temperature generally induced a high structural rejuvenation. In general, the annihilation of free volume is a spontaneous process, and the annihilation rate increases with the temperature. On the other hand, the temperature or thermal fluctuation also facilitates stress-driven ST events, which was verified in the thermo-mechanical creep of high-entropy metallic glasses ($La_{30}Ce_{30}Ni_{10}Al_{20}Co_{10}$) [33]. This finding implies that the thermal activation in STs overwhelms their relaxation, thus resulting in structural rejuvenation. The ΔH_{cp} of the crept glasses at the highest temperature or stress exceeded that of the as-cast sample (orange dashed line).

3.3 Mechanical nanoindentation

We further adopted nanoindentation to examine the mechanical behaviors of rejuvenated and aged glasses after the creeps. The as-cast and pre-annealed samples before creeps were studied again for comparison. Figure 3(a) shows a group of representative load-displacement (P-h) curves of the crept glasses at 643 K ($0.947T_g$). At the fixed P_{max}= 300 mN, a number of rejuvenated glasses can reach a large displacement h of indentation. This finding implies that structural rejuvenation can effectively prompt mechanical softening or plastic deformation. Considering this nonlinear effect, we adopted Meyer's method to calculate hardness [34]:

$$H_V = \frac{P_{max}}{A_t}, \tag{1}$$

where A_t is the true contact area between the indenter and the sample at P_{max}. With the aid of a scanning electron microscope (SEM), A_t can be calculated as $A_t = 3\sqrt{3}\,a^2/4$, where a is the average distance measured from the center of the triangular impression to its corners.

After calculations, we plotted H_V/H_{Vpr} versus σ_{cp}/σ_f in Figure 3(b), where the horizontal dashed line denotes the hardness H_{Vpr} of the pre-annealed sample. This horizontal dashed line can divide the whole plot into the upper softening region and the lower hardening region. The softening glasses were located on the right side of $\sigma_{cp}/\sigma_f=1$ (vertical dashed line) and the hardening ones on the left side. Thus, the softening and hardening samples corresponded to the crept samples at $\sigma_{cp}>\sigma_f$ and $\sigma_{cp}<\sigma_f$, respectively. Combining with the excess relaxation enthalpy in Figure 2(f), we confirmed that the structurally rejuvenated glasses exhibited a mechanical softening behavior, whereas aging led to mechanical hardening. Marked by the soft direction (black arrow), several crept glasses at higher temperature or applied stress were softer than the as-cast sample.

Figure 3(c) presents the residual indentation morphologies of the samples corresponding to those in Figure 3(a). Around the indented areas, several shear bands, which are marked by red boxes, can be observed. This deformation mode is a common feature during the indentation of metallic glasses [35-38]. Compared with the pre-annealed sample, the creep-aged glasses showed more shear bands, whereas shear lo-

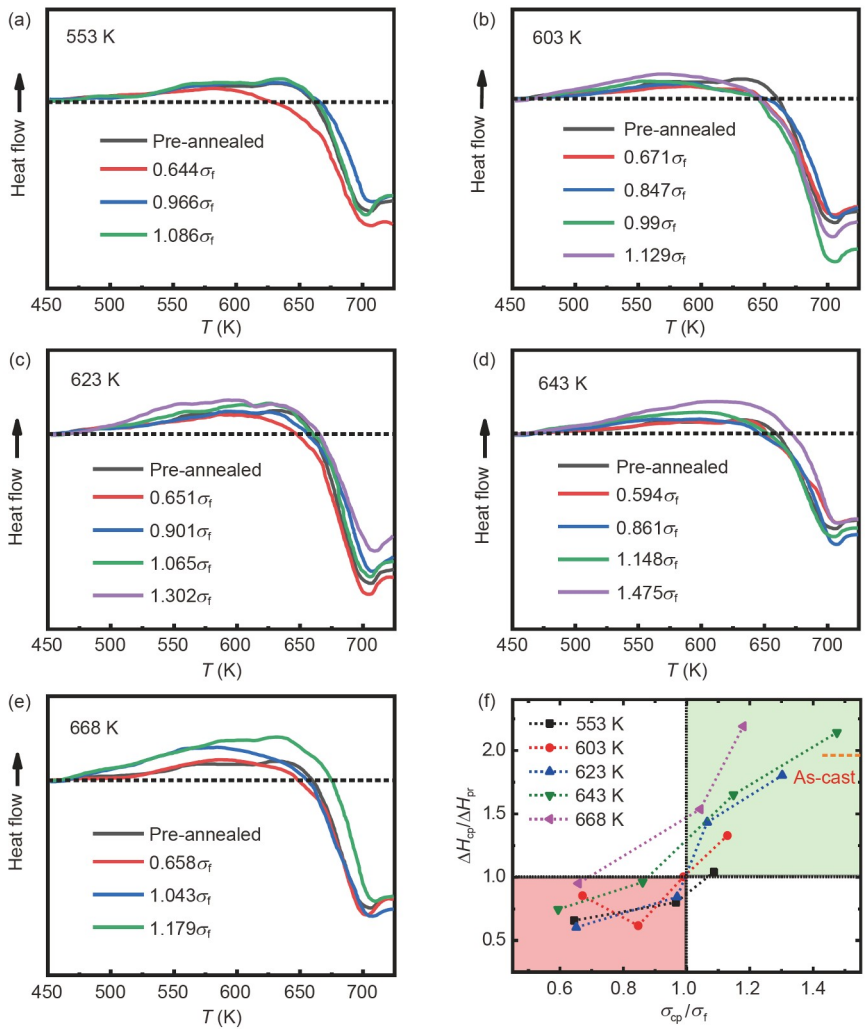

Figure 2 (Color online) Calorimetric measurements: (a)-(e) DSC traces of the crept glasses at 553, 603, 623, 643, and 668 K, respectively, where the pre-annealed samples before creeps were included; (f) plot of $\Delta H_{cp}/\Delta H_{pr}$ versus σ_{cp}/σ_f for all crept glasses.

calization displayed a catabatic trend with increased rejuvenation. The shear banding of the rejuvenated sample at $1.475\sigma_f$ was very similar to that of the as-cast one. The reduction of the shear band number around the indentations signified the recovery of homogeneous plasticity. The observed shear banding behavior was well consistent with the measurements of both relaxation enthalpies in Figure 2(f) and mechanical hardness in Figure 3(b). In the metallic glasses, shear banding resulted from an avalanche of a series of STs [39-45]. Therefore, these results offer solid evidence that structural rejuvenation is associated with complex ST operations of atomic groups and not simply a creation of atomic free volume.

Figure 4 plots the normalized relaxation enthalpy $\Delta H_{cp}/\Delta H_{pr}$ against mechanical hardness $H_V/H_{V\text{pr}}$ for all samples, including the pre-annealed, as-cast, and crept glasses. The enthalpy-hardness correlation exhibited a nearly linear feature regardless of the rejuvenation or aging of glasses. After creeps, the glasses with a high relaxation enthalpy were inclined to present a low mechanical hardness and *vice visa*. Thus, the more rejuvenated glasses were plastically deformed more significantly. As mentioned above, the relaxation enthalpy measures the atomic free volume, whereas the mechanical hardness is closely associated with nanoscale ST events. Therefore, the observed enthalpy-hardness correlation in Figure 4 further indicates that free volume and STs were highly interactive during the present glass creeps.

4 Modeling and analysis

In this section, we performed theoretical modeling of the creep experiments (Figure 1). The modeling is based on the constitutive theory in the unifying framework of STs and free volume [29]. Through modeling, we can analyze the underlying mechanism for glass rejuvenation or aging. Furthermore, the threshold stress σ_c of structural rejuvenation and flow stress σ_f can be quantitatively predicted, which was

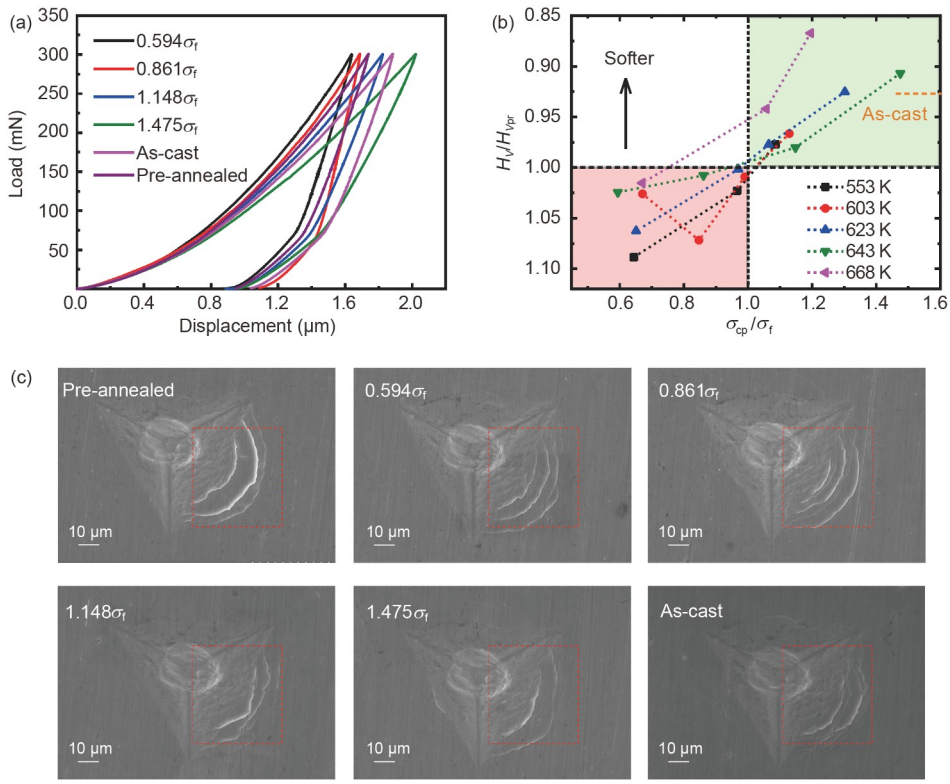

Figure 3 (Color online) Nanoindentation and residual indent morphologies: (a) loading/unloading curves of the glasses after creeps at 643 K, where the as-cast and pre-annealed samples were included for comparison; (b) plot of $H_V/H_{V\mathrm{pr}}$ versus $\sigma_{\mathrm{cp}}/\sigma_{\mathrm{f}}$ for all crept glasses; (c) SEM images of indentation morphologies, where shear bands can be observed in the red dotted box.

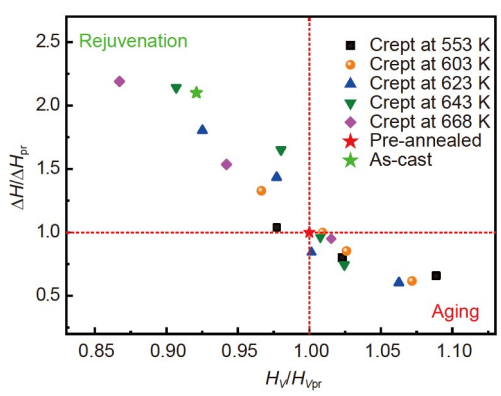

Figure 4 (Color online) Correlation between $\Delta H_{\mathrm{cp}}/\Delta H_{\mathrm{pr}}$ and $H_V/H_{V\mathrm{pr}}$ of all samples.

tested by experimental creep data.

4.1 Theoretical modeling for glass creep

The constitutive theory developed by Jiang et al. [29] describes the homogeneous deformation of amorphous solids. Considering the simple shear case, the total strain was decomposed into elastic and plastic portions, $\dot{\varepsilon} = \dot{\varepsilon}^{\mathrm{el}} + \dot{\varepsilon}^{\mathrm{pl}}$. The elastic strain obeys Hooke's law, $\varepsilon^{\mathrm{el}} = \sigma/\mu$, where σ is the applied shear stress and μ is the shear modulus. The plastic deformation results from a cascade of ST operations that only switch forth and back between shear "positive" and "negative" directions. Here, the activation rate of two-state STs depends on the combined effect of applied stress, thermal fluctuation, and local free volume. The dynamic balance of two-state STs determines the plastic strain rate:

$$\dot{\varepsilon}^{\mathrm{pl}} = \exp\left(-\frac{1}{\xi}\right)\exp\left[E_{\mathrm{A}}\left(1-\frac{1}{T}\right)\right]\left[\Lambda\sinh\left(\frac{\sigma}{T}\right) - \Delta\cosh\left(\frac{\sigma}{T}\right)\right], \tag{2}$$

where ξ is the average concentration of free volume, T is the temperature, and E_{A} is the thermal activation energy of STs. Δ and Λ are the internal state variables of the system, representing the bias and summation of normalized populations of two-state STs, respectively. For the creep test, the shear stress was kept constant. In addition, isothermal treatment was adopted, and the temperature rise was expected to be negligible because of extremely low strain rates. Physically, the applied shear stress and resulting plastic flow will constantly reconstruct the two-state STs, thus creating and destroying local configurations. Given the action of plastic work, the dynamic evolution of two-state ST populations can be expressed as follows:

$$\dot{\Delta} = 2\dot{\varepsilon}^{\mathrm{pl}} - \varphi\,|\sigma\dot{\varepsilon}^{\mathrm{pl}}|\,\Delta, \tag{3}$$

$$\dot{\Lambda} = \varphi\,|\sigma\dot{\varepsilon}^{\mathrm{pl}}|\,(1-\Lambda), \tag{4}$$

where φ is a dimensionless coefficient. The free volume dynamics, including its generation and annihilation, was also considered. Here, the net creation of free volume depends on the competition between the ST-induced creation and relaxation-mediated annihilation [31]. This finding is different from the single-atom-jump-based free volume dynamics developed by Spaepen [46]. Therefore, the net creation of the free volume can be calculated as follows:

$$\dot{\xi} = D_{ia}|\sigma\dot{\varepsilon}^{\mathrm{pl}}| - \phi\exp\left(-\frac{1}{\xi}\right)\exp\left[E_{\mathrm{a}}\left(1-\frac{1}{T}\right)\right]. \quad (5)$$

The first term on the right-hand side describes the ST-induced creation of free volume, which can be estimated by considering the conversion of a fraction of the plastic work into the bulk energy. The variable D_{ia} refers to the dilatancy factor measuring the free volume creation capability of a system. The last term accounts for the annihilation, which mainly relies on thermal transformations of STs. The parameter ϕ is a coefficient that characterizes the efficiency of depleting free volume, and E_{a} is the energy barrier of annihilation. According to atomistic simulations [47], E_{A} and E_{a} are the energy barriers corresponding to the two processes of the configurational rearrangement, namely, the climb to the saddle point and fall into a minimum, respectively. Therefore, E_{A} and E_{a} are unequal, where the former is generally larger than the latter [48]. The current constitutive model can describe not only the creep experiment with a constant stress but also the constant strain-rate test and a natural aging process. For example, in the absence of shear stress, the dynamics of Δ and Λ freeze and the system undergoes a spontaneous time-logarithmic free-volume annihilation process.

The simulated glass creeps were carried out to verify the rationality of this model. The mechanical and physical parameters of $Zr_{55}Cu_{30}Ni_5Al_{10}$ metallic glass were selected: μ=32 GPa, ϕ=10, and φ=0.5. Accordingly, eqs. (2)-(5) can be numerically integrated at a fixed stress and temperature for an initial system. The selected initial system was as follows: Λ_0=0.6, Δ_0=0.01, D_{ia}=0.009, E_{A}=3.83 eV, E_{a}=0.4 eV, and ξ_0=0.055. We generalized the present simple shear stress state to the uniaxial stress state and then conducted a quantitative comparison with the uniaxial creeps. Figure 5 shows the creep strains, including the sudden elastic response and subsequent plastic strain under the constant σ_{cp}, at different stress levels and 0.947T_{g} (643 K). The well-fitted results between experiments and simulations indicated that the present model could properly describe the creep deformation of metallic glasses.

Experimentally, thermo-mechanical creeps have verified that the flow stress σ_{f} can act as the rejuvenation threshold stress. To unravel the underlying mechanism of the threshold stress, we calculated the dynamic evolution of complex STs and free volume under different constant stresses (Figure 6). Here, the increased rate of STs is defined as $Cr_{\Lambda} = \partial\dot{\Lambda} / \partial\Lambda$. Figure 6(a) shows that Cr_{Λ} has several orders of magnitude differences under different stress levels, indicating that STs have similar fingerprints but different dynamics [49]. Evidently, STs were increasingly activated with the increase in stress, leading to different evolutions of free volume (Figure 6(b)). For the $\sigma_{\mathrm{cp}}<\sigma_{\mathrm{f}}$ creep, the insufficient activation of STs led to the annihilation of free volume, which in turn hindered further STs. Thus, Cr_{Λ} decreased slightly, although the

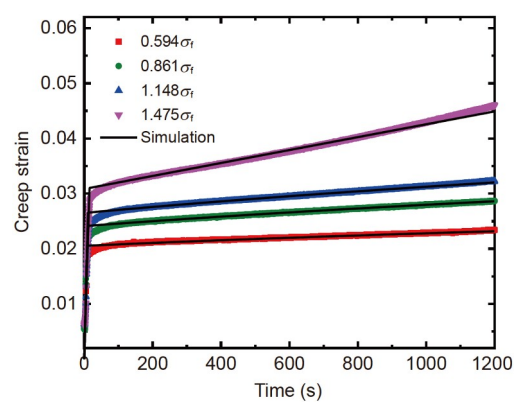

Figure 5 (Color online) Comparison between experimental (color scatters) and simulated (black lines) creep strains vs. loading time at 0.947T_{g} under different applied stresses.

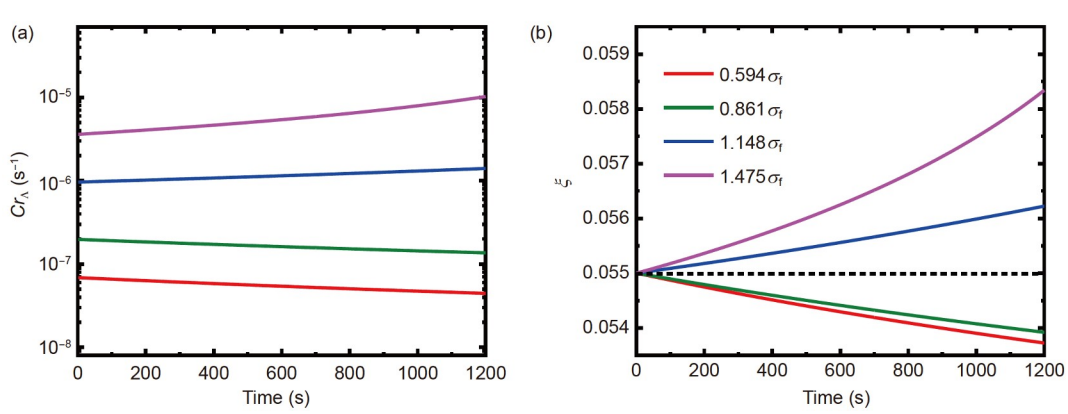

Figure 6 (Color online) Dynamic evolution of (a) ST rate and (b) free volume under creeps at 0.947T_{g}.

external stress remained constant. On the contrary, a continuous creation of free volume was observed for the $\sigma_{cp}>\sigma_f$ creep, which further promoted ST events and induced the gradual increase in Cr_Λ under constant stress [50]. Therefore, the structural rejuvenation characterized by the excess free volume is controlled by stress-driven STs for glass creeps.

In addition, the activation of STs gave rise to macroscopic plastic strain. In Figure 1, the green and red solid curves represent the creep-rejuvenated and creep-aged strain, respectively. A strain threshold was also observed between rejuvenated and aged samples, which is in accordance with previous works [23,51-53]. We also noticed that several curves were very close, although they belonged to different groups. These curves may be near the boundary between rejuvenation and aging. Beyond σ_f or threshold stress σ_c, different strain responses implied the transition of deformation mode from jammed to flowing. From a potential energy landscape perspective, the rejuvenation process involves β- and α-relaxations, which correspond to the configurational hopping into higher energy and disorder states across a series of subbasins and megabasins, respectively [54,55]. Therefore, the study on rejuvenation also provides a new window into understanding the elusive plastic yielding of metallic glasses [56-58]. For the crept glasses below σ_f or σ_c, the feedback between STs and free-volume dynamics was negative, thus contributing to continuous structural relaxation or aging.

4.2 Stress boundary between rejuvenation and aging

Theoretically, how to construct this temperature-dependent stress boundary must be determined. To attain this objective, we derived the analytical expressions of σ_c and σ_f based on the present model. At σ_f or σ_c, the competition between the ST-induced creation of free volume and relaxation-mediated annihilation reached a balance. Therefore, we approximately have $\dot{\xi}=0$, $\Lambda=\Lambda_0$, $\Delta=\Delta_0$ when the creep stress is σ_c. According to eqs. (2) and (5), the relationship between threshold stress σ_c and temperature can be obtained as follows:

$$\left[\sigma_c\Lambda_0\sinh\left(\frac{\sigma_c}{T}\right)-\sigma_c\Delta_0\cosh\left(\frac{\sigma_c}{T}\right)\right]\exp\left[(E_A-E_a)\left(1-\frac{1}{T}\right)\right]=\frac{\phi}{D_{ia}}. \tag{6}$$

The value of σ_c decreases with increasing temperature, revealing that STs are easily activated at high temperatures for the creeps [23,59]. Similarly, previous results revealed a great number of flow units at high temperatures, easily activating a high number of STs [33]. Thus, the crept glasses at high temperatures possess a high relaxation enthalpy (Figure 2(f)), which may exceed that of the as-cast sample. This viewpoint was also verified by the result of high-pressure annealing [60].

The homogeneous flow behavior was analyzed to derive the analytical expression of σ_f. In a constant strain-rate experiment, the shear stress was determined by $\dot{\sigma}=\mu(\dot{\varepsilon}-\dot{\varepsilon}^{pl})$. Here, we normalized the stress by $\sigma_0=2k_BT_g/V_a$ and strain by $\varepsilon_0=n_\infty V_a$, where k_B is Boltzmann constant, V_a is the ST activation volume, and n_∞ is the total populations of STs in a steady-flow state [29]. The normalized stress and strain are denoted as σ' and ε', respectively. Figure 7 presents the normalized stress-strain curve and the corresponding free volume evolution during the deformation. Similar to typical amorphous solids, a stress overshoot and the following softening behavior normally occur in the plastic flow [61-65]. The stress first increased to the peak stress σ_p and then decreased to its final steady-state value σ_f. Correspondingly, the free volume decreased slightly and then increased gradually until it approached saturation. The stress overshoot is a signal for the production of free volume. On the contrary, in several special cases without peak stress and overshoot, the free volume only exhibits the annihilation dynamics [8,62,66]. Therefore, we affirmed that a stress higher than σ_f is an effective trigger for the structural rejuvenation of glasses.

Under the steady-state flow stress σ_f, the free volume approaches its saturation, and we have $\dot{\xi}=0$. In addition, the two-state STs approach their respective saturation, resulting in the following:

$$\dot{\Delta}=0,\ \dot{\Lambda}=0. \tag{7}$$

In this case,

$$\Lambda\to 1,\ \ \Delta\to\frac{2}{\varphi\sigma_f}. \tag{8}$$

Combining eqs. (2), (5), and (8) yields the following expression for σ_f:

$$\left[\sigma_f\sinh\left(\frac{\sigma_f}{T}\right)-\frac{2}{\varphi}\cosh\left(\frac{\sigma_f}{T}\right)\right]\exp\left[(E_A-E_a)\left(1-\frac{1}{T}\right)\right]=\frac{\phi}{D_{ia}}. \tag{9}$$

The steady-state flow stresss σ_f also decreases with the

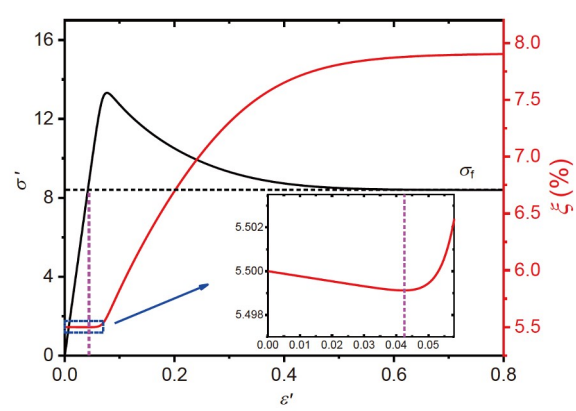

Figure 7 (Color online) Normalized stress-strain curve with a strain rate of 1.6×10^{-4} s^{-1} at T=0.947T_g and the corresponding evolution of free volume dynamics. The inset is the close-up of the blue dotted region.

increase in temperature. Figure 7 shows that σ_f (black dashed line) is very close to σ_c, which corresponds to the minimum of free volume (inset). Eqs. (6) and (9) have similar forms and approximate values (Figure 8). They provide the temperature dependence of σ_c and σ_f, which are used to construct the stress boundary between structural rejuvenation and physical aging, respectively.

To draw the diagram of the rejuvenation boundary for the comparison of experimental and numerical results, we normalized the stresses by their respective peak stress. Experimentally, flow and peak stresses can be easily obtained in the stress-strain curves shown in sect. I of Supporting Information. In addition, the creep stresses were normalized by the peak stress. With respect to numerical results, the analytical expressions of σ_c and σ_f were known, but σ_p was not analytical due to the uncertainty of STs and free volume. Therefore, we carried out simulated constant strain-rate tests at different temperatures to obtain σ_p as shown in sect. IV of Supporting Information.

Figure 8 intuitively shows the stress boundary between creep-induced rejuvenation and aging over a wide range of temperatures. In the panel, the green hexagons represent the creep-rejuvenated samples, whereas red circles represent the creep-aged ones. The shapes are always separated by the blue stars (experimental data of flow stress). Meanwhile, the experimental flow stress can be well fitted by numerical flow stress (pink dashed line) or threshold stress (black dashed line). Based on this boundary, the map can be divided into a creep-rejuvenated green region and a creep-aged red region. The gradation of color denotes the degree of rejuvenation or aging, which was also verified by the results in Figure 2(f). Figure 8 delineates the high-stress-induced rejuvenation and low-stress-induced aging of metallic glasses in thermo-mechanical creep.

By extrapolating the map, the normalized threshold stress at ambient temperature was about 0.8-0.9, which is consistent with the results of elastostatic compression in

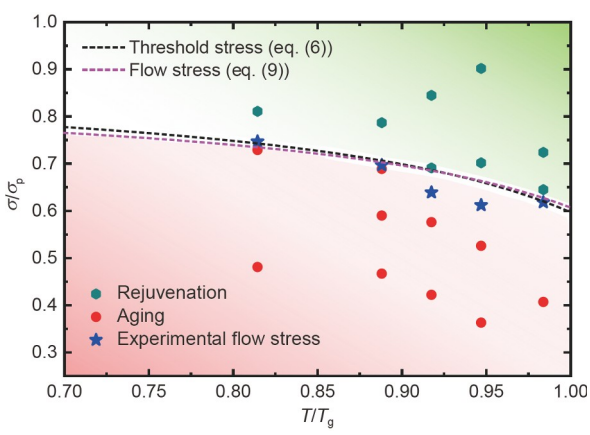

Figure 8 (Color online) Phase diagram of stress boundary between creep-rejuvenated (green) and creep-aged (red) regions in $Zr_{55}Cu_{30}Ni_5Al_{10}$ metallic glass.

$Zr_{35}Ti_{30}Be_{27.5}Cu_{7.5}$ metallic glasses [28]. Meanwhile, at temperatures slightly below T_g, the normalized critical stress that activated STs was about 0.4-0.5 [54], which also agrees with the present predictions. Thus, the essential condition of rejuvenation at sub-T_g is the activation of β- and α-relaxations induced by stress higher than its threshold. However, in the supercooled liquid region, α-relaxation will also be thermally activated in the absence of stress. In this situation, fast quenching will also lead to structural rejuvenation, in which the non-affine strain can be frozen [67]. Therefore, the key to structural rejuvenation is the activation and reconstruction of STs, accompanied by the accumulation of non-affine strain.

5 Conclusion

The stress boundary between structural rejuvenation and aging was systematically investigated via experimental thermo-mechanical creeps in a typical Zr-based metallic glass. Using DSC and nanoindentation, we carried out the structural and mechanical characterizations of crept samples, respectively. Relaxation enthalpy and mechanical hardness showed that structural rejuvenation always occurs only when the creep stress exceeds a threshold that is numerically approximate to the steady-state flow stress. The theoretical constitutive model based on the framework of STs and free volume was adopted to uncover the mechanism of the observed stress threshold. Beyond this stress threshold, the generation of free volume induced by explosive STs overwhelms its annihilation, leading to structural rejuvenation; otherwise, this step gives rise to aging. This mechanism can be used to explain most of the mechanical or thermo-mechanical rejuvenation methods, such as elastostatic loading [68], high-pressure torsion [25], cryogenic thermal cycling [69], and high temperature creep [23]. However, several exceptions, such as ion irradiation, were observed because such rejuvenation is due to the direct increase in free volume induced by injected ions [70].

Furthermore, we deduced the analytical expressions of threshold and flow stresses. Both construct the stress boundary between rejuvenation and aging, as verified by the experimental creep data. This work not only provides useful implications for optimizing the mechanical properties of metallic glasses but also deepens our understanding of the structural rejuvenation of glasses.

This work was supported by the National Outstanding Youth Science Fund Project (Grant No. 12125206), the National Natural Science Foundation of China (Grant Nos. 11972345, and 11790292), and the NSFC Basic Science Center for "Multiscale Problems in Nonlinear Mechanics" (Grant No. 11988102).

Supporting Information

The supporting information is available online at http://phys.scichina.com

and https://link.springer.com. The supporting materials are published as submitted, without typesetting or editing. The responsibility for scientific accuracy and content remains entirely with the authors.

1 P. G. Debenedetti, and F. H. Stillinger, Nature **410**, 259 (2001).
2 W. H. Wang, Prog. Mater. Sci. **106**, 100561 (2019).
3 A. L. Greer, Science **267**, 1947 (1995).
4 T. C. Hufnagel, Nat. Mater. **14**, 867 (2015).
5 Y. Sun, A. Concustell, and A. L. Greer, Nat. Rev. Mater. **1**, 16039 (2016).
6 M. C. Ri, D. W. Ding, Y. H. Sun, and W. H. Wang, J. Mater. Sci. Tech. **69**, 1 (2021).
7 M. Jiang, Sci. China-Phys. Mech. Astron. **63**, 106131 (2020).
8 J. Pan, Y. P. Ivanov, W. H. Zhou, Y. Li, and A. L. Greer, Nature **578**, 559 (2020).
9 K. W. Park, C. M. Lee, M. Wakeda, Y. Shibutani, M. L. Falk, and J. C. Lee, Acta Mater. **56**, 5440 (2008).
10 Y. Wu, H. Bei, Y. L. Wang, Z. P. Lu, E. P. George, and Y. F. Gao, Int. J. Plast. **71**, 136 (2015).
11 Y. Tong, W. Dmowski, Y. Yokoyama, G. Wang, P. K. Liaw, and T. Egami, Scripta Mater. **69**, 570 (2013).
12 W. Song, X. Meng, Y. Wu, D. Cao, H. Wang, X. Liu, X. Wang, and Z. Lu, Sci. Bull. **63**, 840 (2018).
13 B. Shang, W. Wang, A. L. Greer, and P. Guan, Acta Mater. **213**, 116952 (2021), arXiv: 2012.01105.
14 H. Zhou, R. Hubek, M. Peterlechner, and G. Wilde, Acta Mater. **179**, 308 (2019).
15 J. Pan, Y. X. Wang, Q. Guo, D. Zhang, A. L. Greer, and Y. Li, Nat. Commun. **9**, 560 (2018).
16 A. Das, E. M. Dufresne, and R. Maaß, Acta Mater. **196**, 723 (2020).
17 L. Zhang, Y. Wu, S. Feng, W. Li, H. Zhang, H. Fu, H. Li, Z. Zhu, and H. Zhang, J. Mater. Sci. Tech. **38**, 73 (2020).
18 M. Q. Jiang, W. H. Wang, and L. H. Dai, Scripta Mater. **60**, 1004 (2009).
19 F. Jiang, M. Q. Jiang, H. F. Wang, Y. L. Zhao, L. He, and J. Sun, Acta Mater. **59**, 2057 (2011).
20 M. Q. Jiang, G. Wilde, and L. H. Dai, Scripta Mater. **127**, 54 (2017).
21 Y. Z. Lu, M. Q. Jiang, X. Lu, Z. X. Qin, Y. J. Huang, and J. Shen, Phys. Rev. Appl. **9**, 014023 (2018), arXiv: 1706.06229.
22 G. Ding, C. Li, A. Zaccone, W. H. Wang, H. C. Lei, F. Jiang, Z. Ling, and M. Q. Jiang, Sci. Adv. **5**, eaaw6249 (2019).
23 Y. Tong, W. Dmowski, H. Bei, Y. Yokoyama, and T. Egami, Acta Mater. **148**, 384 (2018).
24 Y. Tong, T. Iwashita, W. Dmowski, H. Bei, Y. Yokoyama, and T. Egami, Acta Mater. **86**, 240 (2015).
25 W. Dmowski, Y. Yokoyama, A. Chuang, Y. Ren, M. Umemoto, K. Tsuchiya, A. Inoue, and T. Egami, Acta Mater. **58**, 429 (2010).
26 A. D. Phan, A. Zaccone, V. D. Lam, and K. Wakabayashi, Phys. Rev. Lett. **126**, 025502 (2021), arXiv: 2007.15524.
27 W. Zhu, J. Liu, S. Mao, and X. Wei, J. Mech. Phys. Solids **146**, 104216 (2021).
28 M. Zhang, Y. M. Wang, F. X. Li, S. Q. Jiang, M. Z. Li, and L. Liu, Sci. Rep. **7**, 625 (2017).
29 M. Q. Jiang, G. Wilde, and L. H. Dai, Mech. Mater. **81**, 72 (2015).
30 B. G. Yoo, J. Y. Kim, Y. J. Kim, I. C. Choi, S. Shim, T. Y. Tsui, H. Bei, U. Ramamurty, and J. Jang, Int. J. Plast. **37**, 108 (2012).
31 A. Lemaître, Phys. Rev. Lett. **89**, 195503 (2002), arXiv: cond-mat/0108442.
32 P. Cao, M. P. Short, and S. Yip, Proc. Natl. Acad. Sci. **114**, 13631 (2017).
33 L. T. Zhang, Y. J. Duan, D. Crespo, E. Pineda, Y. J. Wang, J. M. Pelletier, and J. C. Qiao, Sci. China-Phys. Mech. Astron. **64**, 296111 (2021).
34 J. Jang, B. G. Yoo, Y. J. Kim, J. H. Oh, I. C. Choi, and H. Bei, Scripta Mater. **64**, 753 (2011).
35 H. Huang, M. Jiang, and J. Yan, J. Alloys Compd. **754**, 215 (2018).
36 F. Meng, K. Tsuchiya, K. Seiichiro Ii, and Y. Yokoyama, Appl. Phys. Lett. **101**, 121914 (2012).
37 A. L. Greer, Y. Q. Cheng, and E. Ma, Mater. Sci. Eng.-R-Rep. **74**, 71 (2013).
38 W. Jiang, G. Fan, F. Liu, G. Wang, H. Choo, and P. Liaw, Int. J. Plast. **24**, 1 (2008).
39 M. Q. Jiang, and L. H. Dai, J. Mech. Phys. Solids **57**, 1267 (2009).
40 Y. Chen, M. Q. Jiang, and L. H. Dai, Int. J. Plast. **50**, 18 (2013).
41 M. Q. Jiang, G. Wilde, J. H. Chen, C. B. Qu, S. Y. Fu, F. Jiang, and L. H. Dai, Acta Mater. **77**, 248 (2014).
42 F. Van Loock, L. Brassart, and T. Pardoen, Int. J. Plast. **145**, 103079 (2021).
43 R. T. Qu, S. J. Wu, S. G. Wang, X. D. Wang, and Z. F. Zhang, J. Mech. Phys. Solids **138**, 103922 (2020).
44 R. T. Qu, Z. Q. Liu, G. Wang, and Z. F. Zhang, Acta Mater. **91**, 19 (2015).
45 R. T. Qu, S. G. Wang, X. D. Wang, Z. Q. Liu, and Z. F. Zhang, Scripta Mater. **133**, 24 (2017).
46 F. Spaepen, Acta Metall. **25**, 407 (1977).
47 J. Ding, L. Li, N. Wang, L. Tian, M. Asta, R. O. Ritchie, and T. Egami, Mater. Today Phys. **17**, 100359 (2021).
48 M. Heggen, F. Spaepen, and M. Feuerbacher, J. Appl. Phys. **97**, 033506 (2005).
49 D. Şopu, X. Yuan, F. Moitzi, F. Spieckermann, X. Bian, and J. Eckert, Appl. Mater. Today **22**, 100958 (2021).
50 Z. Lv, C. Yuan, H. Ke, and B. Shen, J. Mater. Sci. Tech. **69**, 42 (2021).
51 D. J. Lacks, and M. J. Osborne, Phys. Rev. Lett. **93**, 255501 (2004).
52 D. Fiocco, G. Foffi, and S. Sastry, Phys. Rev. E **88**, 020301 (2013), arXiv: 1302.6518.
53 P. Wang, and X. Yang, Comput. Mater. Sci. **185**, 109965 (2020).
54 J. S. Harmon, M. D. Demetriou, W. L. Johnson, and K. Samwer, Phys. Rev. Lett. **99**, 135502 (2007).
55 W. L. Johnson, and K. Samwer, Phys. Rev. Lett. **95**, 195501 (2005).
56 Y. Huang, J. C. Khong, T. Connolley, and J. Mi, Int. J. Plast. **60**, 87 (2014).
57 Y. Jin, P. Urbani, F. Zamponi, and H. Yoshino, Sci. Adv. **4**, eaat6387 (2018), arXiv: 1803.04597.
58 G. Biroli, and P. Urbani, Nat. Phys. **12**, 1130 (2016), arXiv: 1601.06724.
59 P. Cao, M. P. Short, and S. Yip, Proc. Natl. Acad. Sci. **116**, 18790 (2019).
60 C. Wang, Z. Z. Yang, T. Ma, Y. T. Sun, Y. Y. Yin, Y. Gong, L. Gu, P. Wen, P. W. Zhu, Y. W. Long, X. H. Yu, C. Q. Jin, W. H. Wang, and H. Y. Bai, Appl. Phys. Lett. **110**, 111901 (2017).
61 X. C. Tang, T. Nguyen, X. H. Yao, and J. W. Wilkerson, J. Mech. Phys. Solids **141**, 104023 (2020).
62 J. Lu, G. Ravichandran, and W. L. Johnson, Acta Mater. **51**, 3429 (2003).
63 J. S. Harmon, M. D. Demetriou, W. L. Johnson, and M. Tao, Appl. Phys. Lett. **90**, 131912 (2007).
64 P. de Hey, J. Sietsma, and A. van den Beukel, Acta Mater. **46**, 5873 (1998).
65 J. F. Li, J. Q. Wang, X. F. Liu, K. Zhao, B. Zhang, H. Y. Bai, M. X. Pan, and W. H. Wang, Sci. China-Phys. Mech. Astron. **53**, 409 (2010).
66 V. Srivastava, S. A. Chester, N. M. Ames, and L. Anand, Int. J. Plast. **26**, 1138 (2010).
67 M. Wakeda, J. Saida, J. Li, and S. Ogata, Sci. Rep. **5**, 10545 (2015).
68 H. B. Ke, P. Wen, H. L. Peng, W. H. Wang, and A. L. Greer, Scripta Mater. **64**, 966 (2011).
69 S. V. Ketov, Y. H. Sun, S. Nachum, Z. Lu, A. Checchi, A. R. Beraldin, H. Y. Bai, W. H. Wang, D. V. Louzguine-Luzgin, M. A. Carpenter, and A. L. Greer, Nature **524**, 200 (2015).
70 K. Sun, G. Wang, Y. W. Wang, H. C. Chen, L. Yan, S. Pauly, Y. H. Wu, H. Weber, Q. Wang, B. Huang, Y. D. Jia, J. Yi, and Q. J. Zhai, Scripta Mater. **180**, 34 (2020).